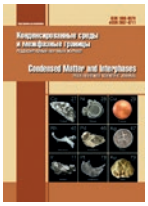

ISSN 1606-867X (Print)
ISSN 2687-0711 (Online)
Condensed Matter and Interphases
Kondensirovannye Sredy i Mezhfaznye Granitsy
https://journals.vsu.ru/kcmf/

Original articles

Research article
https://doi.org/10.17308/kcmf.2025.27/12809

Analysis of anisotropic heat and thermal diffusivity of thermally expanded graphite

D. A. Prokhorov[1,2]✉, M. G. Rybin[3], S. M. Zuev[1,2]

[1]MIREA - Russian Technological University,
78 Vernadsky av., Moscow 119454, Russian Federation

[2]SSC RF FSUE NAMI - State Scientific Center of the Russian Federation Federal State Unitary Enterprise Central Scientific Research Automobile and Automotive Engines Institute,
2 Avtomotornaya st., Moscow 125438, Russian Federation

[3]RUSGRAFEN LLC,
15 Biologov av., Moscow Region, Serpukhov urban district, Obolensk settlement 142279, Russian Federation

Abstract

Purpose: This paper aims to look into the anisotropic thermal diffusivity of thermally expanded graphite (TEG) foil using flash method. Its structure is compared with graphene oxide (GO) multilayer foil. Morphology, diffractogram and surface profilometry of TEG and GO produced by two different manufacturing processes are demonstrated. TEG was made of intercalated graphite by thermolysis, and GO was made by microwave-assisted graphite oxide peeling (MEGO).

Experimental: The paper studies temperature distribution in the TEG sample as a result of continuous exposure to laser radiation and compares it to those of copper and aluminum samples.

Conclusions: It also provides a perspective on possible application of TEG in heat transfer.

Keywords: Two-dimensional allotropic modification of carbon, Graphene, Thermally expanded graphite, Anisotropy, Cooling

For citation: Prokhorov D. A., Rybin M. G., Zuev S. M. Analysis of anisotropic heat and thermal diffusivity of thermally expanded graphite. *Condensed Matter and Interphases*. 2025;27(2): 284–292. https://doi.org/10.17308/kcmf.2025.27/12809

Для цитирования: Прохоров Д. А., Рыбин М. Г., Зуев С. М. К анализу анизотропной тепло- и температуропроводности терморасширенного графита. *Конденсированные среды и межфазные границы*. 2025;27(2): 284–292. https://doi.org/10.17308/kcmf.2025.27/12809

✉ Dmitriy A. Prokhorov,, e-mail: prohorovdmitrii97@yandex.ru

1. Introduction

The aim of this research is to measure the anisotropic physical properties of TEG, in particular thermal and thermal diffusivity, and its practical application. The obtained structure of TEG is compared with that of GO, also studied in the frame of this research. Jackie Renteria et al. [1] carried out orthotropy studies on GO and found a significant difference in GO thermal conductivity values of 61 W/m·K in the in-plane direction and 0.09 in the perpendicular (vertical) direction. Further reduction of the oxygen content in GO by high-temperature treatment up to a temperature of plus 1000 °C in theoretical calculations leads to a value of the thermal conductivity coefficient of about 500 W/m·K. Graphene is superior in its thermophysical properties to metals such as copper and aluminum which ensures its applicability in heat dissipation devices like air and liquid cooling radiators.

Mass production of GO is currently carried out by chemical methods such as vapor deposition and subsequent deposition of graphene on the substrate, oxidation of graphite and subsequent reduction from graphene oxide in liquid, application of surfactants (surfactants) in graphite layering, etc. The GO under study was produced by *GRAFENOX LLC* using the modified Hummers' method. [2] The thickness of the GO is about 10 μm.

Mass production of TEG was carried out by *Silur LLC* from intercalated graphite by thermolysis. Natural, clearly crystalline (coarsely flaked) graphite was used as a starting material whose interlayer space was filled with sulfite ions (intercalants) in the presence of sulfuric acid H_2SO_4. Then the oxidized graphite was heated at a heating rate of at least 600 C°/s to release gaseous decomposition products of H_2SO_4. During the thermal expansion of the intercalated graphite, there was an increase in the size of graphite crystallites along one direction by more than 300 times. The obtained TEG was rolled into thin films with anisotropy maintenance to thicknesses of 0.3 and 1.5 mm.

The paper also provides a comparison of the side surface morphology of the TEG and GO, in contrast to the work of Teddy Tite et al. [3], where the morphology of graphene nanoplates of 1 to 20 nm frontal surface only was considered which does not determine the quality of the overlapping graphene layers.

TEG and GO side surface roughness measurements were performed by optical profilometry. Thermal diffusivity was measured by flash method, which measures the temperature increase of the sample as a function of time using a cadmium-mercury-tellurium (MCT) infrared detector.

To obtain diffractograms, the X-ray diffractometric method was used with the same imaging conditions and slits, a Soller slit was installed both on the X-ray tube side and on the detector side.

Practical studies were carried out based on the results of reaching the maximum temperature in copper and aluminum samples, as well as the sample formed after pressing TEG layers. Throughout the experiment, the temperature change of the samples achieved by laser irradiation was continuously recorded by a thermal imager.

It is well known that ultrahigh pressures affect the interatomic distances in the graphene crystal lattice. The relationship between the Grüneisen parameter and thermal conductivity is described by the Leibfried–Schleman formula (1):

$$\chi = \frac{3}{10\pi^3}\frac{k_B^3 Ma}{h^3\gamma^2}\frac{\theta_D^3}{T} \quad (1)$$

where χ is the heat transfer coefficient (W/m K), θ_D is Debye temperature (K), k_B is the Boltzmann constant ($1.381\cdot10^{-23}$ J/K), M is the molecular weight (kg), h is the Planck's constant ($6.626\cdot10^{-34}$ J/s), a is the lattice parameter (m), T – temperature (K), γ – the Grüneisen parameter.

However, it should be noted that the Grüneisen parameter is more appropriately perceived as a combination of acoustic γ_{ac}, elastic γ_{el}, and thermodynamic γ_{tg} factors whose values together give a difference in the readings from 10 to 15 %. Numerical values for these parameters are given in V. N. Belomestnykh et al. paper [4] and are available for calculation by formulas (2–4):

$$\gamma_{ac} = \frac{9}{2}\frac{x^2 - \frac{4}{3}}{x^2 + 2}, \quad (2)$$

where γ_{ac} is Grüneisen acoustic parameter, x is the parameter characterizing the ratio of propagation

velocity of longitudinal elastic waves to transverse waves.

$$\gamma_{el} = \frac{3}{2}\frac{1+\sigma}{2-3\sigma}, \quad (3)$$

where γ_{el} is the elastic Grüneisen parameter, σ is the Poisson's ratio.

$$\gamma_{tg} = \frac{\alpha V}{\beta_{tg} C_V}, \quad (4)$$

where γ_{tg} is the Grüneisen thermodynamic parameter, α is the thermal expansion coefficient (1/K), β_{tg} is the volumetric compressibility (1/Pa), C_V is the specific heat capacity at constant volume (J/K).

In the course of pressing polycrystalline graphene made by chemical reduction of graphite oxide [5], it was found that without taking into account its anisotropic properties, the thermal conductivity coefficient is about 59 W/m K at the pressing pressure up to 44 MPa. Macroscopically, anisotropy is most clearly manifested in single crystals, but can also be observed in polycrystals, for example, the most stable for boron nitride hexagonal crystal lattice (h-BN) has a layered structure with anisotropic thermal conductivity that ranges from 200 to 500 W/m K in the in-plane direction [6] and up to 30 W/m K in the out-of-plane direction [7].

The cross-sectional plane images of the TEG and GO samples shown in Fig. 1 were made by scanning electron microscopy using an AURIGA CrossBeam scanning electron microscope. As can be seen from Fig. 2, the GO sample has a more oriented arrangement of layers which facilitates the study of its anisotropic properties. However, as the sample thickness equals just about 10 μm, it is not possible to measure the thermal diffusivity with the flash method, at least with the LFA 467 HyperFlash analyzer. For this reason, further thermal diffusivity measurements including anisotropy were performed for the TEG sample.

For TEG, the thermal diffusivity measurement in the in-plane direction was performed by the flash method on an LFA 467 HyperFlash analyzer at various temperatures. In contrast to the hot guard zone (GHP), heat plates (HFM) or thermally stimulated current (TCT) methods,

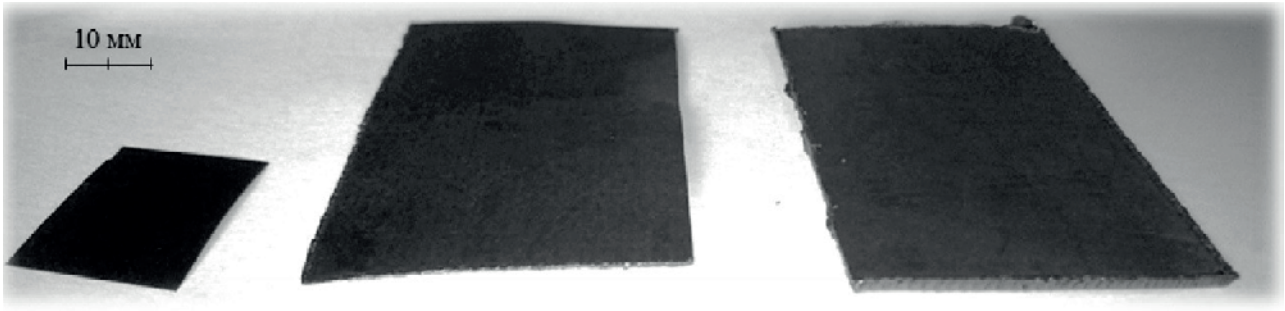

a b c

Fig. 1. TEG and GO samples: a – GO approx. 10 μm thick; b – TEG approx. 0.3 mm thick; c – TEG approx. 1.5 mm thick

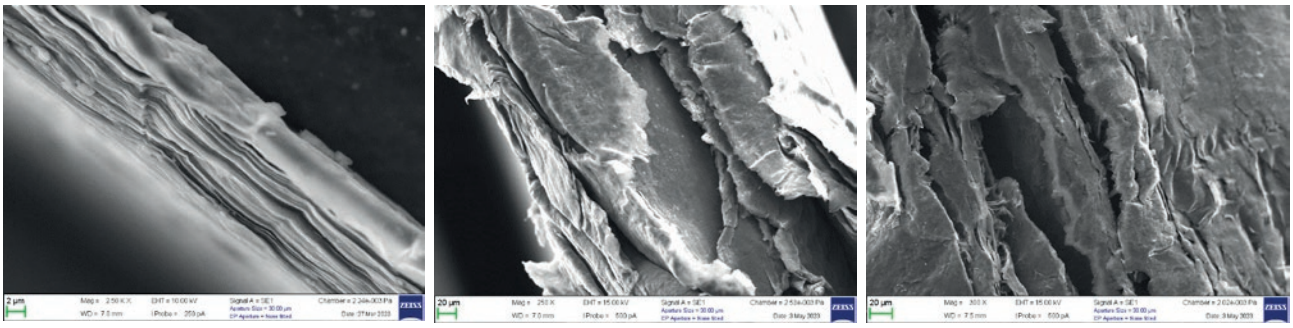

a b c

Fig. 2. Lateral surface morphology of TEG and GO samples: a – GO approx. 10 μm thick; b – TEG approx. 0.3 mm thick; c – TEG approx. 1.5 mm thick

the flash method (LFA) allows the most accurate measurement of thermal diffusivity of the sample in the range of highest values.

Surface roughness of the samples in the cross-sectional plane was determined by arithmetic mean of absolute values of surface deviations from the reference plane *Ra*, RMS value of surface heights (RMS) *Rq*, average maximum profile height (average of ten maximums and ten minimums of the surface) *Rz* and maximum surface height (distance between maximum and minimum of the surface) *Rt*. Surface roughness was created and visualized by optical profilometer WYKO NT 1100 by the non-contact method of optical profilometry.

The diffractograms of the studied samples with a step of 1.2 angular minutes presented in Fig. 3 were obtained by X-ray diffractometric method using X-ray diffractometer DRON-8. On the X-ray tube side, a Soller slit and a 0.5 mm equatorial slit were installed, and on the detector side, a Soller slit, a 0.05 mm equatorial slit, and a nickel beta filter were installed.

For practical studies of temperature distribution in the samples, a unit with a controlled semiconductor laser was assembled whose structure scheme is shown in Fig. 4. The device contains segmental indicators of the current flowing through the semiconductor laser, its voltage, dissipating electric power and temperature in the laser spot. The unit's main control device is a microcontroller with power management technology (picoPower). A USB-UART interface converter with an integrated clock generator and an initial reset circuit at power-on (Power-On Reset) made on a chip base was used as a linking device between the microcontroller and a personal computer. An analog-to-digital converter was used to measure the amount of current and voltage flowing through the laser. The value of current flowing through the laser was constant and amounted to 1 A at a voltage of 4.6 V. To measure the temperature in the laser spot (sample surface) a Fluke Ti125 thermal imager was used in addition to the thermocouple.

2. Experimental

Thermal diffusivity coefficient α of the TEG sample was measured by placing it a cuvette whose bottom surface was heated by pulses of 0.6 ms with radiant energy of 10 J produced by a xenon lamp. The cuvette made of aluminum was specifically designed for layered samples or composites to measure thermal diffusivity in different directions. Subsequently, the sample diffusivity was extracted from the layered cuvette-sample model using Netzsch Proteus software. This software allows to make certain adjustments following heat loss and changes in the distance from the xenon lamp to the sample inside the measuring chamber. Measurements were performed after the sample was thermostated for 60 minutes at constant temperatures of +25 °C, +100 °C and + 150 °C. The time interval τ between pulses (shots) was 7 minutes, and there were

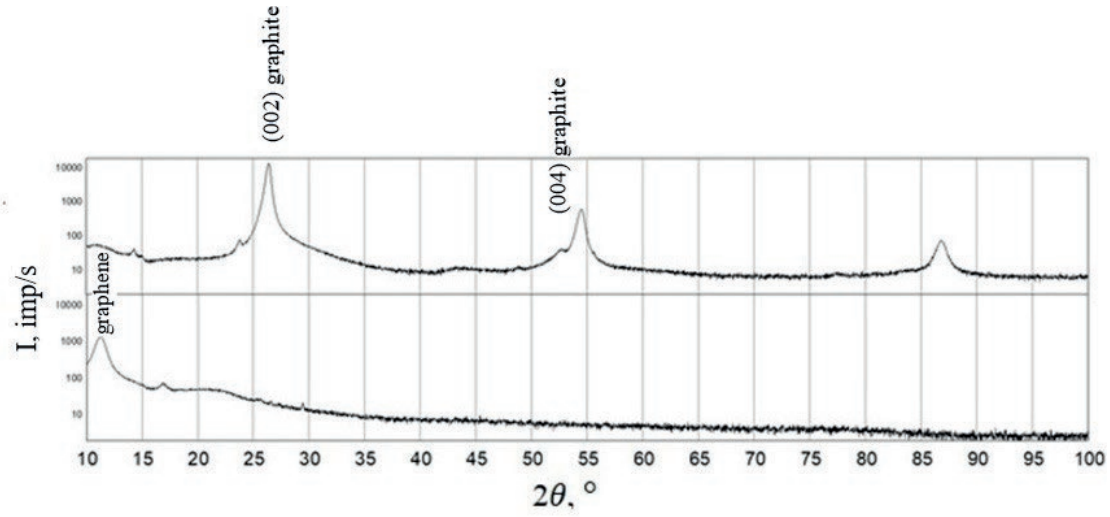

Fig. 3. Diffractograms of TEG and GO samples: top – TEG; bottom – GO

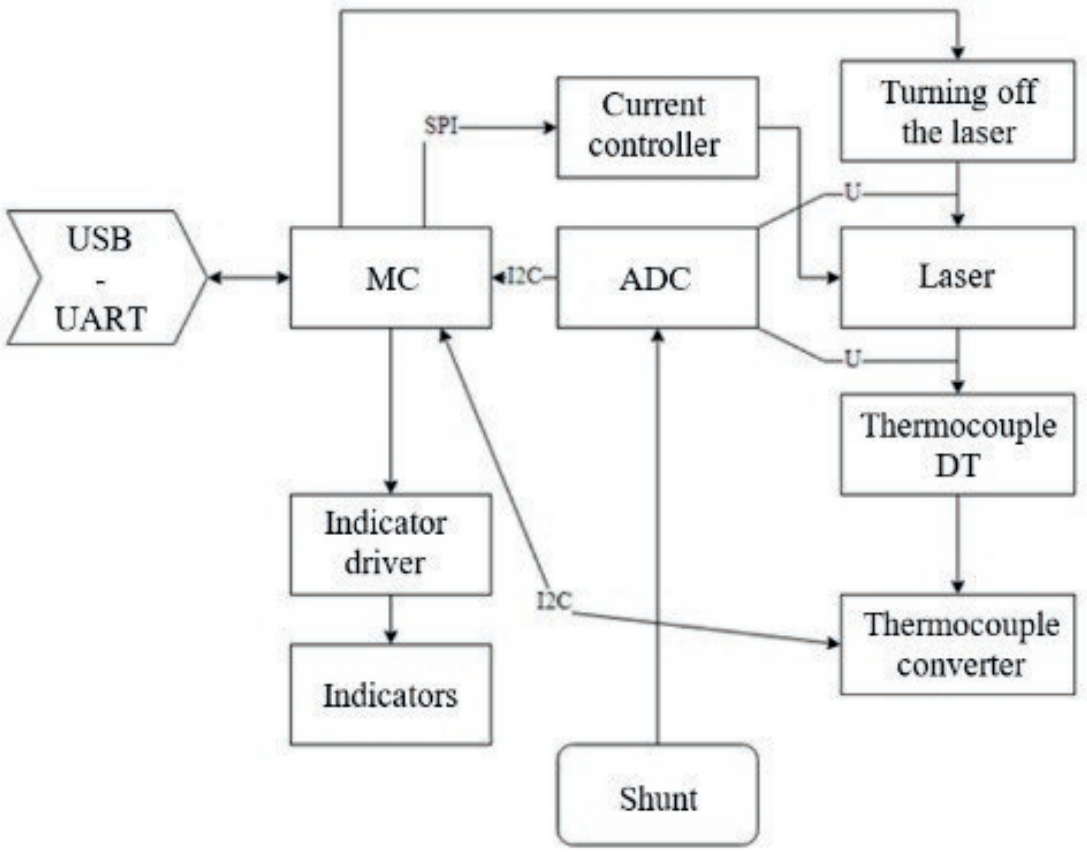

Fig. 4. Structural diagram of controlled semiconductor laser unit

between 10 and 20 of them in order to obtain the average of the measured value. The density of samples ρ was determined after preliminary thermostatization of the sample in vacuum by direct measurements of the sample geometric dimensions and its mass. Heat capacity was determined by differential scanning calorimetry using a DSC 204 F1 calorimeter where both the sample and the reference (AXM-5Q graphite) are maintained at an equal and constant temperature. Value of the heat transfer coefficient was calculated using formula 5 under the assumption of a homogeneous system:

$$\chi(T) = \alpha(T) \cdot \rho(T) \cdot C_p(T) \quad (5).$$

Where ρ is the sample density (kg/m^3), α is the diffusion coefficient (m/s^2), C_p is specific heat capacity at constant pressure (J/kg K).

Based on diffractograms shown in Fig. 3, crystallite sizes of the samples can be roughly estimated using Scherrer equation 6:

$$d = \frac{k\lambda}{\beta \cos\theta} \quad (6),$$

where d is the mean size of coherent scattering regions (nm), k is the sample particle shape factor, λ is the X-ray wavelength (nm), β is half-height reflex width (°), θ is the diffraction angle (°).

Scanning electron microscopy method not only helps to define layer orientation as was shown in Fig. 2, but also to confirm its polycrystalline structure. For samples under study, the morphology of the frontal surface, the characteristic sizes of crystallites obtained by this method were defined (also see Fig. 5).

For practical studies of temperature distribution in the sample, a controlled semiconductor laser was used. The TEG sample was previously compressed under pressure of 300 MPa to a cubic shape with a side of 1.5 cm. The pressing was performed on a hydraulic press by a single impact on 105 layers of the sample which inevitably led to layer compaction and a change in the Grüneisen parameter γ and, consequently, in thermal conductivity coefficient χ. The obtained sample shown in Fig. 6 was placed at a distance of 10 cm from the radiation source as shown in

Fig. 7. After 30 seconds of continuous exposure of the sample to laser radiation, the maximum value of its temperature was recorded. A larger value of thermal conductivity coefficient χ and thermal diffusion α of the sample resulted in a larger maximum temperature T_{max}. To compare the obtained results, two samples of copper and aluminum similar in shape and size were also used.

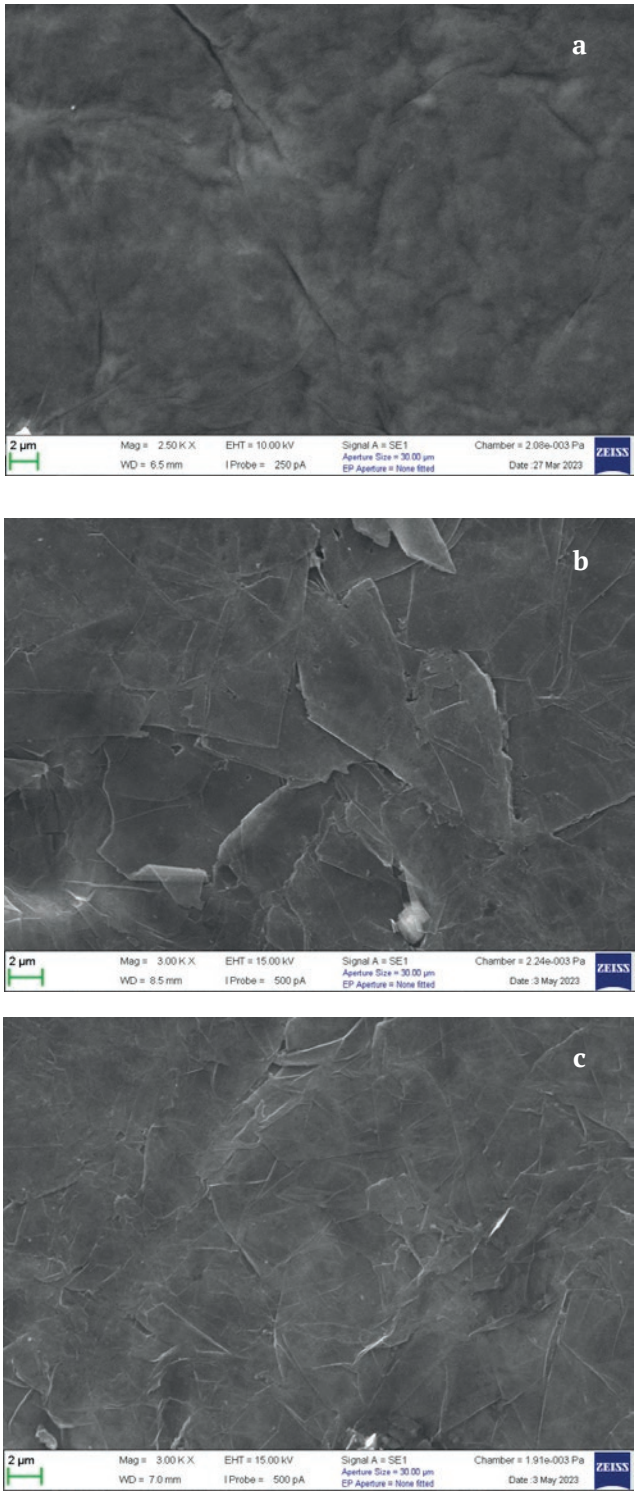

Fig. 5. Frontal surface morphology of TEG and GO samples: a – GO approx. 10 µm thick; b – TEG approx. 0.3 mm thick; c – TEG approx. 1.5 mm thick

3. Results and discussion

Table 1 shows the results of measurements and calculations of physical properties of the TEG sample under study.

A temperature increase in copper, aluminum and silver from + 27 to + 127 °C results in a thermal conductivity coefficient decrease by 2 % [12, p. 70] for copper and by 1.3 % [12, p. 76] for silver, yet in a thermal conductivity coefficient increase by 1 % [12, p. 108] for aluminum. As Table 1 shows, an increase in the TEG temperature at almost similar temperatures (from + 25 °C to + 150 °C) leads to an increase in thermal conductivity by 3 %, but it should be noted that in order to obtain a qualitative dependence of temperature on the TEG thermal conductivity coefficient, it is necessary to increase the number of measurements to several dozens. On average, thermal conductivity of the TEG sample exceeds that of silver by almost one third in the investigated temperature range. It is worth

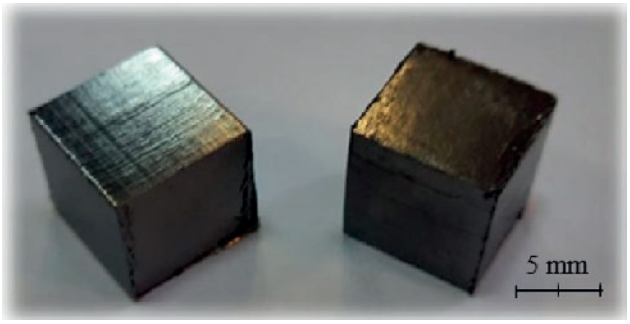

Fig. 6. TEG sample compressed at 300 MPa

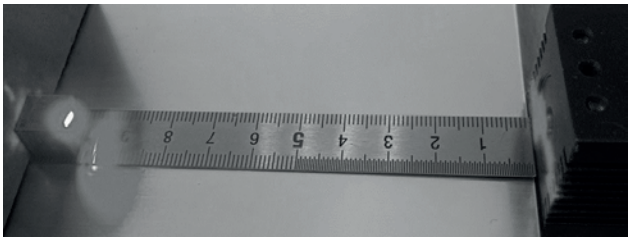

Fig. 7. Experimental conditions for studying temperature distribution in samples under laser irradiation

Table 1. Physical property measurements of TEG sample

ρ, kg/m³	α, mm²/s	χ, W/(m·K)	*T*, °C
990	116.75±δ_α	622.8±δ_χ	plus 25
	81.94±δ_α	597.4±δ_χ	plus 100
	66.37±δ_α	642.6±δ_χ	plus 150

* δ_α – relative error of thermal diffusivity measurement 3 % [8] or ± 8 % [9].

** δ_χ – relative error of thermal conductivity measurement 4 % [8, 10] or 10.5 % [9, 11], calculated on the basis of the total error according to formula (5) with negligibly small density measurement error (approx. 0.2 %)

noting that the change in thermal conductivity of TEG in the studied temperature range is more pronounced. When the temperature of copper, aluminum and silver increases from + 27 to + 127 °C their thermal conductivity decreases by 5 % [12, p. 70], 2 % [12, p. 76], and 0.2 % [12, p. 108], respectively, whereas the TEG conductivity decreases by 43 % at almost similar temperatures.

The side surface roughness of the compressed TEG sample whose 2D relief images are shown at various resolutions in Fig. 8, does not require further processing before use in heat transfer.

Measuring the the TEG and GO surface morphology allowed to determine a polycrystalline structure with crystallite interfaces.

Table 2 shows the results of calculations for diffractograms of TEG and GO samples shown in Fig. 3. The TEG sample has a peak near 26.55° (Fig. 3) corresponding to the graphite phase with orientation (002) [14], and a peak near 54.69° with orientation (004). The peaks in the regions of 23° to 25° and 42° to 45° may correspond to both graphite and graphene phases. The diffractogram of the GO sample has one intense peak in the region of angle 11°. Based on earlier studies of graphene diffractograms [15–17], it can be concluded that the diffractogram of the TEG sample corresponds to that of graphite, yet it is impossible to reliably conclude that graphene is absent in it. The diffractogram of the GO sample corresponds to the diffractogram of grapheme without any graphite content.

When studying temperature distribution in the TEG sample compressed under continuous exposure to laser radiation, the thermogram was obtained as shown in Fig. 9. As a result of continuous exposure to laser radiation for 30

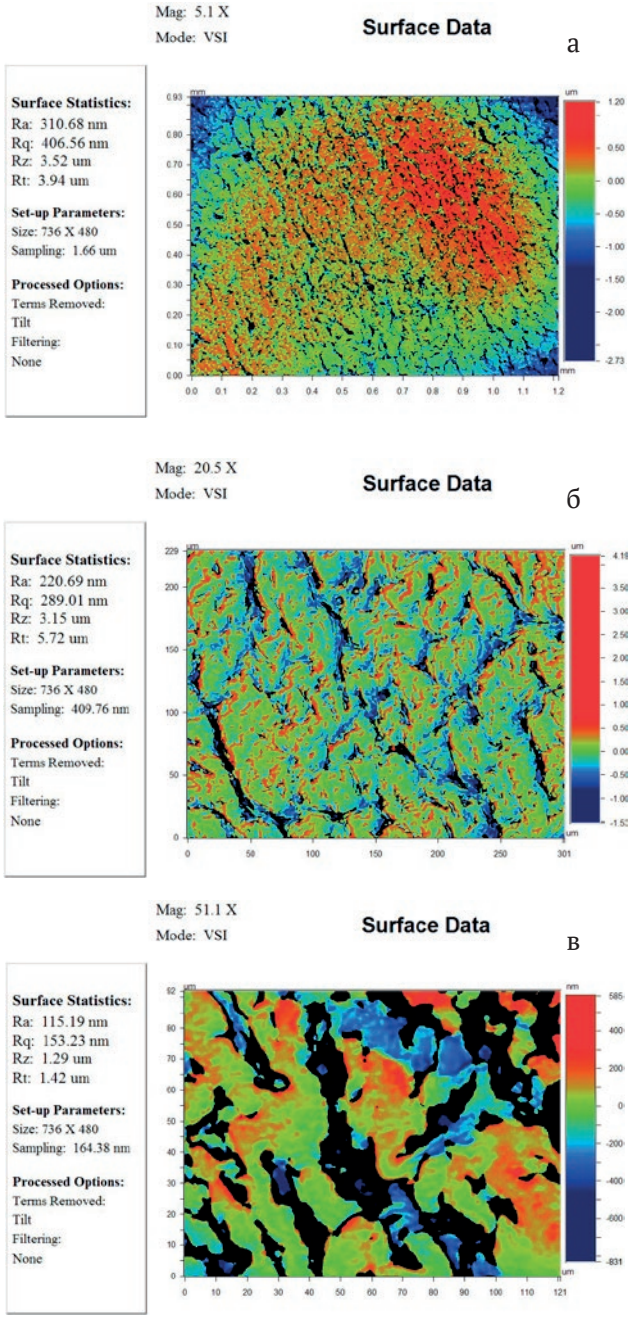

Fig. 8. Side surface roughness of compressed TEG sample at different resolutions: a – 5.1 X; b – 20.5 X; c – 51.1 X

seconds, the maximum temperature of +31.2 °C was recorded in this sample, while in similar samples of copper and aluminum it was +29.0 °C and +28.4 °C, respectively.

4. Conclusions

Application of anisotropic properties of TEG in the in-plane direction allows to increase thermal conductivity by an order of magnitude

Table 2. Results of calculations based on diffraction patterns of the studied samples

Образец	*K*	*a*, nm	2θ, °	β, °	*d*, nm
Fig. 2b	0.94	$0.1541\pm\Delta_{\alpha}$	$26.41\pm\Delta_{\theta}$	0.4356	19.57
Fig. 2a	0.94	$0.1541\pm\Delta_{\alpha}$	$11.24\pm\Delta_{\theta}$	1.2644	6.59

* Δ_{α} absolute measurement error of crystal lattice parameter lattice parameter 0.0001 nm [13].
** Δ_{θ} – absolute error of diffraction angle measurement 0.01 % [13].

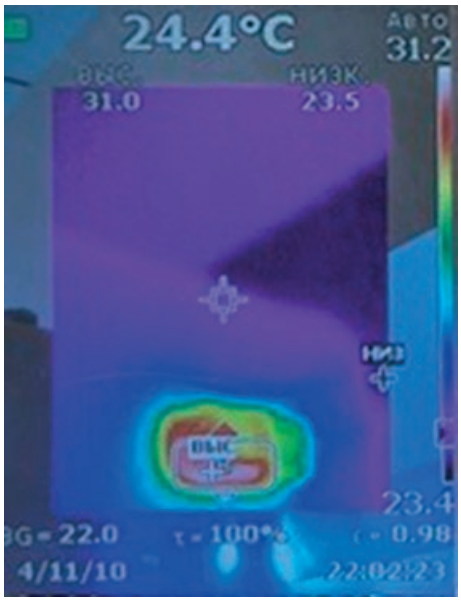

Fig. 9. Thermogram of temperature distribution in compressed TEG sample exposed to continuous laser irradiation

which allows for its application as a material replacing copper in heat spreading covers (IHS), simplest cooling radiators, and thermal interfaces (TIM).

Some of the features limiting TEG application include its high conductivity of electric current, and problems in using it for making complex shaped structures.

Although it is impossible to measure thermal diffusivity of the GO sample with the flash method, at least with the LFA 467 HyperFlash analyzer, due to its thickness of about 10 μm, thermophysical properties of this sample may be superior to those of the TEG sample. It is possible to make similar measurements for the GO sample by pressing multiple GO samples at high pressures (up to several GPa).

Contribution of the authors

The authors contributed equally to this article.

Conflict of interests

The authors declare that they have no known competing financial interests or personal relationships that could have influenced the work reported in this paper.

References

1. Renteria J. D., Ramirez S., Malekpour H., … Balandin A. A. Anisotropy of thermal conductivity of free-standing reduced graphene oxide films annealed at high temperature. *Advanced Functional Materials*. 2015;25(2): 4664. https://doi.org/10.1002/adfm.201501429

2. Shulga Y. M., Baskakov S. A., Baskakova Y. V., … Kovalev I. D. Supercapacitors with graphene oxide separators and reduced graphite oxide electrodes. *Journal of Power Sources*. 2015;279: 722–730. https://doi.org/10.1016/j.jpowsour.2015.01.032

3. Tite T., Chiticaru E. A., Burns J. S., Ionita M. Impact of nano-morphology, lattice defects and conductivity on the performance of graphene based electrochemical biosensors. *Journal of Nanobiotechnology*. 2019;17(101): p. 5. https://doi.org/10.1186/s12951-019-0535-6

4. Belomestnykh V. N., Tesleva E. P. Poisson's ratio and Gruneisen parameter of solids. *Bulletin of Tomsk Polytechnic University*. 2003;306(5); 8–12. (In Russ., abstract in Eng.). Available at: https://elibrary.ru/htnczd

5. Prokhorov D. A., Zuev S. M. Investigation of the characteristics of a graphene-based thermal interface for cooling integrated microcircuits. *Protection of Metals and Physical Chemistry of Surfaces*. 2023;59(2): 155–162. https://doi.org/10.1134/s2070205123700247

6. Donghua L., Xiaosong C., Yaping Y., … Dacheng W. Conformal hexagonal-boron nitride dielectric interface for tungsten diselenide devices with improved mobility and thermal dissipation. *Nature Communications*. 2019;10(1188): 2. https://doi.org/10.1038/s41467-019-09016-0

7. Sarkarat M., Lanagan M., Ghosh D., Lottes A., Budd K., Rajagopalan R. Improved thermal conductivity and AC dielectric breakdown strength of silicone rubber/BN composites. *Composites Part C: Open Access*. 2020;2: 100023. https://doi.org/10.1016/j.jcomc.2020.100023

8. Light-flash-apparatus LFA 467 HyperFlash-Series methods, techniques, applications for temperature and warmth factors. Netzsch. 0823. Available at: https://analyzing-testing.netzsch.com/_Resources/Persistent/3/6/7/f/367f54b9bc7fc3a5b36f6b41191f5dbaf802ecb7/LFA_467_HyperFlash_en_web.pdf

9. *Description of the type of measuring instrument. Thermophysical parameter meters of the LFA 467 HyperFlash modification* / GCSI SI FSUE "VNIIM named after

D. I. Mendeleyev"*. Certificate of approval of the type of measuring instrument No. 57491-14. 2022. (In Russ.)

10. *Technical Specifications DSC 204 F1 Phoenix* / Netzsch. 0222. Available at: https://analyzing-testing.netzsch.com/_Resources/Persistent/b/8/6/c/b86c2a6637064b1361d580c2bc05367072b194d6/Key_Technical_Data_en_DSC_204_F1_Phoenix.pdf

11. *Description of the measuring instrument type. Differential scanning calorimeters of the DSC 200 F3, DSC 204 F1, DSC 204 HP, DSC 404 C, DSC 404 F1, DSC 404 F3 modifications* / GCSI SI FSUE "VNIIM named after D. I. Mendeleyev"*. Certificate of approval of the type of measuring instruments No. 54912-13. 2023. (In Russ.)

12. Zinoviev V. E. *Thermophysical properties of metals at high temperatures**. Reference ed., Moscow: Metallurgy Publ.; 1989. p. 384. (In Russ.)

13. *Description of the type of measuring instrument. X-ray diffractometers of the DRON- model 8N and DRON-8T* / GCSI SI FSUE "VNIM named after D. I. Mendeleev"*. Certificate of approval of the type of measuring instruments No. 82575-21. 2023. (In Russ.)

14. Fayos J. Possible 3D carbon structures as progressive intermediates in graphite to diamond phase transition. *Journal of Solid State Chemistry*. 1999;148(2): 278–285. https://doi.org/10.1006/jssc.1999.8448

15. Siburian R., Sihotang H., Lumban S. R., Supeno M., Simanjuntak C. New route to synthesize graphene nano sheets. *Oriental Journal of Chemistry*. 2018;34(1): 182–187. https://doi.org/10.13005/ojc/340120

16. Fentaw T. E., Worku D. A. Controlled synthesis, characterization and reduction of graphene oxide: a convenient method for large scale production. *Egyptian Journal of Basic and Applied Sciences*. 2017;4(1): 74–79. https://doi.org/10.1016/j.ejbas.2016.11.002

17. Aftab A., Sadeeq U., Abrar K., … Qipeng Y. Graphene oxide selenium nanorod composite as a stable electrode material for energy storage devices. *Applied Nanoscience*. 2020;10: 1243–1255. https://doi.org/10.1007/s13204-019-01204-0

** Translated by author of the article*

Information about the authors

Dmitriy A. Prokhorov, postgraduate student of the Department of Optical-Electronic Devices and Systems, MIREA - Russian Technological University, Chief Specialist of FSUE "NAMI", (Moscow, Russian Federation).

prohorovdmitrii97@yandex.ru

Maksim G. Rybin, Cand. Sci. (Phys.–Math.), Deputy General Director for Science, Rusgrafen LLC (Moscow Region, Serpukhov Urban District, Obolensk settlement, Russian Federation).

https://orcid.org/0000-0003-1529-5326

rybin@rusgraphene.ru

Sergei M. Zuev, Cand. Sci. (Phys.–Math.), Associate Professor, Associate Professor of the Department of Optical-Electronic Devices and Systems, MIREA - Russian Technological University, Head of Department of FSUE "NAMI", (Moscow, Russian Federation).

https://orcid.org/0000-0001-7033-1882

sergei_zuev@mail.ru

Received 04.08.2024; approved after reviewing 30.01.2025; accepted for publication 17.02.2025; published online 25.06.2025.